Mesoporous Silica Films for Sensing Volatile Organic Compounds using Attenuated Total Reflection Spectroscopy

Bettina Baumgartner, Jakob Hayden and Bernhard Lendl

Research Division of Environmental Analytics, Process Analytics and Sensors, Institute of Chemical Technologies and Analytics, Technische Universität Wien, Getreidemarkt 9, 1060 Vienna, Austria

Abstract

Sensitivity of evanescent wave sensing of gaseous species can be vastly increased by enrichment materials that locally concentrate the analyte on the sensor. Here, we investigate functionalized mesoporous silica films as versatile enrichment layer for sensing volatile organic compounds (VOCs) from gas-phase. Attenuated total reflection (ATR) crystals were coated with silica films of different pore sizes and their capability to enrich three different aromatic hydrocarbons from a vapor stream was studied by means of Fourier Transform infrared (FTIR) spectroscopy. Thereby, single-digit ppmv limits of detection (LOD) were achieved with an effective path length of only 6.3 µm. The selectivity introduced by the functionalization of the silica films effectively minimized interferences of water vapor, which gave access to the spectral fingerprint region between 1550 and 1450 cm^{-1}. This allowed to discriminate and quantify toluene, *p*-xylene and 1,2,4-trimethylbenzene in multicomponent mixtures at high humidity. Fast response and regeneration times and enrichment factors up to 32 000 showcase the high potential of this material for evanescent wave sensing.

Keywords: Mid-IR Spectroscopy, Mesoporous Materials, Sensing, Volatile Organic Compounds, Functional Coating

1. Introduction

Volatile organic carbons (VOCs) typically originate from combustion processes, paints and inks, fuel products, or farming. Their harmful effects on human health and environment demand for continuous monitoring, especially for indoor environments where their concentration levels were reported up to ppm-levels.[1,2,3,4] An increasing awareness for environmental protection and personal safety has fueled the development of a broad spectra of VOC sensors based on i) photo-ionization detectors (PID)s, (ii) electrochemical sensors, (iii) metal oxide sensors, (iv) UV spectrometers, or (v) micro-gas chromatographs.[5] However, these sensors are either not selective, interfere with other compounds found in air (e.g. NO, NO_2 or CO interfere with metal oxide sensors) or are bulky and expensive, as it is the case of chromatographs. Therefore, it is still challenging to detect VOCs at low concentration from a complex atmosphere.

With respect to selectivity, FTIR spectroscopy has proven a great candidate as it probes the characteristic vibrations of the molecule in the fingerprint region of the spectrum.[6] However, high sensitivity in IR spectroscopy demands for long interaction path lengths, which are typically realized using multi-pass cells.[7] Due to their large size and high cost, this approach is not applicable for compact and low-cost sensors. Sensing in the evanescent field, e.g. using attenuated total reflection (ATR) fibers or waveguides with small diameter such as silver halide fibers, can potentially overcome these limitations.[8–10] For example, hollow core waveguides allow for sensitivity enhancement of up to 60 % per meter optical path length compared to multi-pass gas cells.[11] In particular, the great advances in the field of integrated optics of the past decades hold promise to achieve the functionality and advantages of conventional IR spectroscopic chemical sensing, but at a drastically reduced foot-print and lower cost due to CMOS-fabrication.[12] Fully functional spectrometers have been reported with the size of a few cm^2, with interaction pathlenghts comparable with silver halide fibers.[13–17] Different integrated sensing schemes based on micro-cavity resonators,[18] mid-infrared (IR) spectroscopy[19], mid-IR dual comb spectroscopy,[20] Raman spectroscopy,[21,22] or photothermal spectroscopy[23] have been demonstrated. Despite their impressive integration of functionality, achieving effective optical path lengths of several meters as routinely used in spectroscopic gas sensing is challenging in the near-IR and even harder in the mid-IR. Here, the path length is limited by the waveguide losses that are still > 1 dB/cm for Ge-on-SOI or graded GeSi waveguides suitable for the mid-IR. [24–27] Despite the shorter path length and in contrast to multi-pass cells, sensitivity can be increased using enrichment claddings that attract and hence concentrate the analyte within the volume probed by the evanescent wave. In addition, these claddings can introduce

additional selectivity e.g. hydrophobicity to exclude the strong IR absorber water. This concept was proven on ATR crystals and optical fibers coated with polymers,[28–30], mesoporous silica,[31,32] zeolites,[33,34] or metal oxides[35] to detect VOCs in gas or aqueous phase. While limits of detection (LODs) at the ppb-level for VOCs in aqueous phase and low ppm levels for the gas phase have been reached for polymer coatings, they lack in terms of adhesion to the ATR element and response time due to long diffusion times. Zeolite coatings have shown a much faster response and strong enrichment. However, these coatings must be regenerated by heating to > 200 °C to fully remove adsorbed molecules and recover the enrichment layer. Here, mesoporous materials stand out compared to microporous materials such as zeolites or activated carbon as they allow fast regeneration without the need of harsh treatments.[36,37] Furthermore, their high porosities of up to 70 % allow for fast diffusion and hence fast response times which was exploited for capacitive, resistive and optical gas sensors.[38] Besides high-surface areas and fast diffusion, mesoporous materials are low refractive index materials (between n=1.3 - 1.03, tunable by functionalization and porosity),[39,40] which is a highly demanded feature for claddings of integrated optics as the refractive index contrast determines the light confinement within a waveguide.[9] Recently, we presented the first steps towards the exploitation of these features for VOC sensing on integrated optics.[41] In addition, silica's rich surface chemistry allows further tuning of selectivity by introducing functional groups, which allow for discriminating different analytes according to characteristics such as size, polarity, or functionality. [36,42,43]

In this contribution we showcase the versatility of mesoporous silica films as enrichment materials for sensing VOCs in gas phase using mid-IR spectroscopy. The enrichment of three VOCs into mesoporous films with three different pore sizes coated on Si ATR crystals was investigated. Using low-cost Si ATR crystals in a commercial FTIR spectrometer enabled the rapid characterization of a variety of mesoporous silica films. Spectral analysis was performed within the region of the ring skeleton vibrations of the aromatic hydrocarbons between 1550 cm^{-1} - 1450 cm^{-1}. This region is usually not accessible in transmission gas measurements due to the strong water vapor bands found between 1900 cm^{-1}- 1350 cm^{-1}. By using functionalized, hydrophobic silica films, quantitative analysis of toluene, *p*-xylene and 1,2,4-trimethylbenzene was performed und yielded single-digit ppmv LODs and enrichment factors > 9000. Fast response and regeneration times within seconds were observed. In addition, quantification of the individual components of multicomponent mixtures in presence of high relative humidity was performed. The achieved selectivity and vastly increased sensitivity with an effective path length of only 6 µm demonstrate the potential of these films for integrated optical sensing.

2. Materials and Methods

2.1. Synthesis of mesoporous films

Tetraethoxysilane (TEOS, Sigma Aldrich 99.5%), abs. ethanol (Fisher, 99.6%), hydrochloric acid (VWR, 37%), cetyltrimethylammonium bromide (CTAB, Sigma Aldrich, 99%), Pluronic F127 and Pluronic P123 (Sigma Aldrich), were used as received.

Mesoporous silica film synthesized using CTAB was prepared as previously reported with a final molar ratio of 1:13:5:5 × 10^{-3}:0.12 for TEOS:EtOH:H_2O:HCl:CTAB.[32] Mesoporous silica films synthesized using F127 and P123 were prepared by stirring of ethanol, TEOS, water and 0.1 M HCl (molar ratio TEOS:EtOH:H_2O:HCl = 1:8.7:10.3:0.01 for F127 and TEOS:EtOH:H_2O:HCl = 1:5.2:6:0.01 for P123) at room temperature for 20 min. A polymer solution was added to the sol giving a final molar ratio of TEOS:EtOH:F127:H_2O:HCl = 1:16:0.01:16.3:0.015 for F127 film and TEOS:EtOH:P123:H_2O:HCl = 1:14.6:0.009:6:0.01: for P123 film. The mixture was stirred for 3 h at room temperature. All three films were spin coated with a spinner velocity of 2000 rpm and subsequently calcined at 400 °C for 4 h with a heating ramp of 1 K min^{-1}. Surface functionalization was realized by immersing the freshly calcined films in 20 mL toluene with 0.5 mL hexamethyldisilazane (HMDS) at reflux temperature for 24 h. The recovered films were rinsed with toluene and acetone and dried at 110 °C over night before use.

2.2. Characterization of films

Low Angle X-ray diffraction data was collected with an Empyrean PANanalytical multipurpose diffractometer in Bragg-Brentano geometry operating with a Cu anode at 45 kV and 40 mA using a GalliPix detector. Samples were placed on the silicon single crystal sample holder. The diffraction patterns were recorded at room temperature between 1° and 5° (2θ) at a rate of 100 s/step and a step size of 0.01°. Film thickness was determined with a Bruker Dektak XTL Stylus profilometer by measuring five scratches distributed over the entire film for several coatings. IR spectra of the films were obtained using an uncoated Si ATR crystal as background.

2.3. Optical setup

Mesoporous silica films were coated on low resistivity Si cut into 20 x 10 x 0.5 mm^3 pieces and the shorter facet was polished with diamond grinding wheels (grain sizes of 15 µm, 9 µm, 3 µm, 1 µm, 0.1 µm) to a defined angle of 45°. This ATR crystal configuration has 20 active bounces and a depth of penetration (per bounce) of ca. 500 nm at 1500 cm^{-1} (n_{Si}=3.42, n_{sample}=1.33).[44] The ATR crystals were inserted into a custom-made mount and fixed with a FKM O-ring and an aluminum gas flow cell with a volume of ca. 4 cm^3 (compare Figure 1). This setup was placed in the sample compartment of a Vertex 80v FTIR spectrometer

(Bruker Optics, Ettlingen, Germany) equipped with an N_2-cooled MCT detector. Spectra were recorded with 2 cm^{-1} resolution and 32 scans were averaged per spectrum (double-sided, backward-forward acquisition mode, 8 s per spectrum). Prior to spectrum acquisition, the spectrometer was flushed with dry air. The noise floor of the system was obtained by means of 100 % lines, i.e. a scan of the N_2 flushed flow cell with a background scan obtained under same conditions, and yielded an root-mean-square noise of $3 \cdot 10^{-5}$ A.U. between 1800 cm^{-1}- 1450 cm^{-1}.

Spectra were analyzed using the software package OPUS 7.5 (Bruker Optics) and spectra processing and fitting was performed in Matlab.

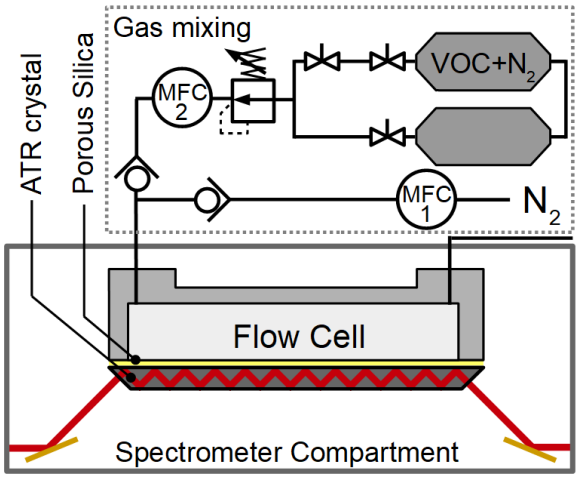

Figure 1: Optical setup and gas mixing and conditioning unit.

Concentrations of the applied VOC vapors were determined from IR transmission measurements. Although concentrations could be derived from the injected liquid volume as well as the gas volume and applied pressure, this approach was found to be less accurate than IR spectroscopy (no precise pressure gauge was available and VOCs were injected with varying losses). A gas cell with ZnSe windows and a path length of 4 cm was used for transmission measurements. For calibration of VOCs concentrations, transmission spectra of each VOC (standards prepared as explained in section 2.4.) were integrated in the C-H stretching region between 3100 cm^{-1} - 2800 cm^{-1}. Concentrations were obtained from the band areas using reference spectra of 1 ppm/m VOC from the PNNL database. Since a reference spectrum of 1,2,4-trimethylbenzene was not available, the spectrum of 1,2,3-trimethylbenzene was used, assuming very similar integrated absorptivity in the analyzed spectral region. The concentration of the dry and humidified gas mixture obtained from 200 µL toluene and *p*-xylene and 100 µL 1,2,4-trimethylbenzene was calculated from band areas at 728 cm^{-1}, 795 cm^{-1} and 805 cm^{-1} for toluene, *p*-xylene and

trimethylbenzene respectively. This region was selected, as the bands in the C H stretching region are unspecific and do not allow for calibration of the individual compounds. Lower signal-to-noise ratio in this region compared to the C-H stretching region results in an increased uncertainty of applied concentrations (~ 0.2 $\%_{rel}$ for single component calibration in C-H stretching region), which is indicated by horizontal error bars in Figure 6.

2.4. Sample preparation

Gas samples were prepared by injecting 200 - 500 µL of liquid VOC into a 10 cm long tubing (6 mm OD) enclosed with two manual valves connected to an evacuated pressure vessel (2 x 10 L, Festo, CRVZS Series, interconnected with stainless steel tubing, see Figure 1). The reservoir was filled with N_2 to 9 bar alternating trough the VOC-filled tubing as well as a second tubing connected to the second vessel to ensure good gas mixing. The reservoir was then connected to a mass flow controller (MFC, Voegtlin AG, Switzerland) using a reducing valve. A second mass flow controller was used for N_2 and both streams were mixed to yield a flow of 1 L min^{-1}. Both MFCs were controlled using LabView. All tubing were PUN or PTFE tubing (6 mm OD). As VOCs diffuse into the tubing and to avoid the carryover of VOCs, the point of mixing both streams was kept as short as possible and was ca. 30 cm. In addition, standard calibration of VOCs in transmission measurements was performed with increasing concentration as well as in random order. For both methods the same concentrations were found, hence, no contamination due to carryover or tubing diffusion is assumed.

3. Results and Discussion

3.1. Characterization of Mesoporous films

Mesoporous silica films were prepared via the evaporation induced self-assembly process using different templates,[32,45,46] namely CTAB, P123 and F127. Sols were prepared by acidic catalyzed condensation of TEOS and template and were spin coated onto Silicon ATR crystals followed by calcination at 400 °C. Thereby, films with pores of different sizes and orders were obtained. Note that surfactant removal can also be achieved by other, low-temperature treatments.[32,47] X-ray diffraction proved the periodic arrangement of the mesoporous films (see ESI). The formation of silica, complete removal of the template and successful surface functionalization was confirmed by FTIR measurements. Bands at 1100 cm^{-1} are associated with Si-O-Si bands, the band at 1258 cm^{-1} is associated with the trimethyl-silane moiety introduced by the functionalization (see ESI). It should be stressed that functionalized mesoporous silica is IR transparent in the fingerprint region 1250 cm^{-1} - 1900 cm^{-1} as no absorption bands are found there.

The pore size distribution of the films was determined as previously reported and yielded pore diameters of 5 nm, 7 nm, and 12.5 nm for the films synthesized using CTAB, P123 and F127, respectively.[48]

3.2. Adsorption of Volatile Organic Compounds

To showcase the capability of mesoporous silica coated ATR crystals to sense VOC, three aromatic hydrocarbons with different saturation pressures were selected: Toluene (p_{sat} = 2.66 kPa), *p*-xylene (p_{sat} = 1.18 kPa) and 1,2,4-trimethylbenzene (p_{sat} = 0.28 kPa) (all values given for 298 K). FTIR-ATR spectra of all three VOCs in liquid phase are given in Figure 2 (orange curves). The bands at 1496 cm^{-1}, 1517 cm^{-1} and 1506 cm^{-1} stem from the skeletal ring vibrations of toluene, *p*-xylene and 1,2,4-trimethylbenzene, respectively. Concentration series between 5 - 800 ppmv were applied to the three different mesoporous films. Figure 3 (black curves) shows exemplarily spectra of toluene, *p*-xylene and trimethylbenzene with 786 ppmv, 787 ppmv and 80 ppmv, respectively, adsorbed into the mesoporous silica film produced using CTAB. Note, due to the adsorption into the film, the skeletal ring vibrations have the same band positions as found in neat spectra (compare black and orange curves). The additional band at 1620 cm^{-1} is associated with the bending vibration of water that is also present in the gas streams as e.g. the respective liquids were not anhydrous and this residual water also adsorbs into the films. The redshift of the bending vibration is a result of the hydrophobic functionalization that largely impede the water molecule's interactions with the surface, which influences the local order of water and hence the water vibrations.[49,50] Due to the hydrophobic surface functionalization of the film with HMDS, this adsorption could be decreased to less than 1 % compared the absorbance of water vapor on pristine mesoporous silica for the same humidity.[46]

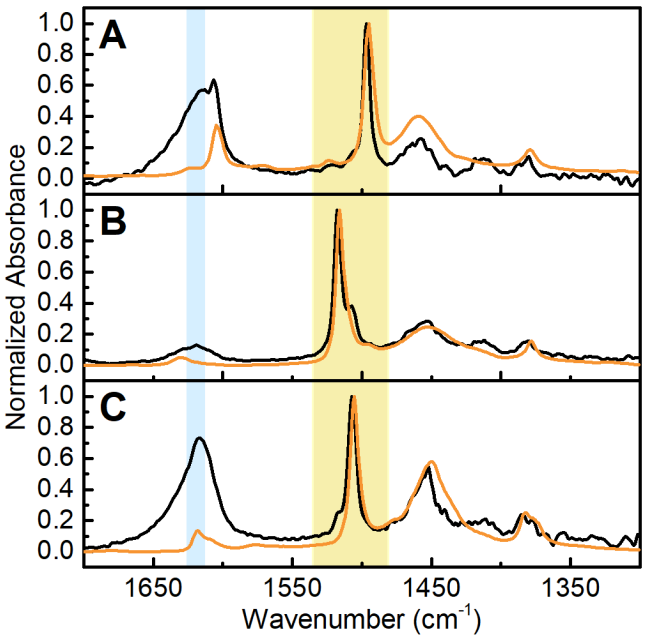

Figure 2: FTIR spectra (normalized to a peak absorbance of 1) of toluene (A), *p*-xylene (B) and 1,2,4-trimethylbenzene (C) obtained after enrichment into the mesoporous silica film synthesized using CTAB (black curves) and for the pure substance on a commercial ATR unit (orange spectra). Bands of adsorbed water are highlighted in blue and the spectral region of interest with skeletal ring vibrations of toluene at 1496 cm^{-1}, *p*-xylene at 1517 cm^{-1} (residuals of trimethylbenzene are visible in the spectrum) and 1,2,4-trimethylbenzene at 1506 cm^{-1} is highlighted in yellow.

The area of Lorentzian profiles fitted to the absorption bands shown in Figure 4 were used for quantitative analysis. The band areas obtained for a concentration series of toluene adsorbed into the mesoporous silica film prepared using CTAB are depicted in Figure 3A. Here, the concentration was increased every minute and spectra were recorded every 10 s. The fast adsorption, hence short response time, was similar for all three VOCs and all three films (see Figure S3 in the ESI for other films and analytes). The complete regeneration of all films was simply achieved by flushing the flow cell with pure N_2 the signal returning back to its initial absorbance within seconds.

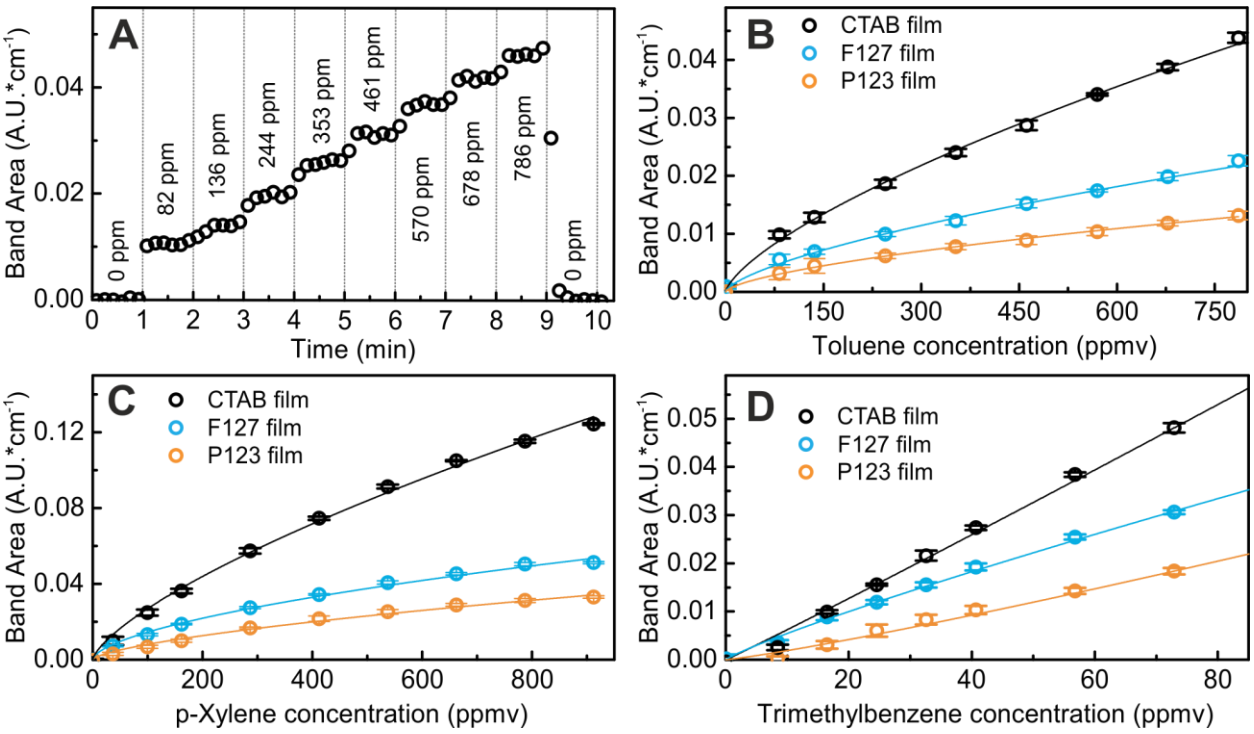

Figure 3. (A) Calibration of the mesoporous silica film prepared using CTAB for toluene. (B-D): Adsorption isotherms of different mesoporous films for (B) toluene, (C) *p*-xylene and (D) 1,2,4-trimethylbenzene.

The band areas for concentration series of all VOCs adsorbed into all three films are given in Figure 3. For all VOCs, the mesoporous silica film prepared using CTAB with smallest pore size shows superior adsorption behavior, followed by the film prepared using F127 and the film synthesized with P123. The calibration functions were described by the Freundlich equation, which describes multilayer adsorption of adsorbates typically found in mesoporous materials:[51]

$$q_e = K_F c^{\frac{1}{n}} \qquad (1)$$

Where, q_e is the amount of adsorbed analyte (corresponding to the obtained band areas in AU cm^{-1}), c is the concentration in the gas (ppmv), K_F (AU cm^{-1} [ppmv]$^{-1/n}$) is the Freundlich affinity coefficient, and n (unitless) is the Freundlich linearity index. Table 1 summarizes the fitted parameters.

Table 1: Calibration function parameters obtained from a fit with the Freundlich equation.

	Analyte	**K_F [AU cm^{-1} (ppmV)$^{-1/n}$]**	***n***
CTAB film	Toluene	$3.9 \cdot 10^{-4}$	1.42
	p-xylene	$1.0 \cdot 10^{-3}$	1.54

	1,2,4-trimethylbenzene	$7.3 \cdot 10^{-4}$	1.01
F127 film	Toluene	$2.47 \cdot 10^{-5}$	1.48
	p-xylene	$4.65 \cdot 10^{-4}$	1.45
	1,2,4-trimethylbenzene	$9.11 \cdot 10^{-4}$	1.19
P123 film	Toluene	$1.91 \cdot 10^{-5}$	1.58
	p-xylene	$3.75 \cdot 10^{-4}$	1.51
	1,2,4-trimethylbenzene	$2.27 \cdot 10^{-4}$	1.01

Due to the low concentrations applied for trimethylbenzene chosen due to its low saturation vapor pressure, an almost linear calibration function was obtained, while for toluene and *p*-xylene the profile flattens out for higher concentrations, which is reflected in higher *n* values. This is due to lower affinity of the analyte to the adsorbate for an increasing number of adsorbed monolayers. For all analytes, relative vapor pressures of $p/p_0 < 0.1$ were applied, which is the region of monolayer formation typically found in gas sorption experiments for mesopores. Within this region, no capillary condensation and, hence, no hysteresis between adsorption and desorption occurs,[51] ensuring reversible sensing.

The obtained calibration functions allow for retrieving the limits of detection (LOD) defined as q_e(LOD)= 3·σ, with σ being the standard deviation derived from consecutive 100 % lines. The LODs for the best performing film are 7 ppm, 6 ppm and 3 ppm for toluene, *p*-xylene and 1,2,4-trimethylbenzene, respectively. To put these LODs into perspective and compare them to transmission measurements, it is interesting to consider the effective optical path length for which these numbers were obtained. We recently introduced the determination of the effective path length $d_{e,eff}$ within the film on an ATR crystal.[32] For the mesoporous silica film prepared with CTAB with a film thickness *th* = 400 nm, $n_{SiO2\text{-}film}$ = 1.13,[46] $n_{Si\text{-}ATR}$ = 3.42, we find $d_{e,eff}$ = 6.3 µm at $\tilde{\nu}$=1500 cm^{-1}. This allows for retrieving an enrichment factor defined as the ratio between the band area A_{ATR} obtained from ATR spectra and simulated band areas $A_{transmission}$ one would obtain for the same path length $d_{e,eff}$ based on reference spectra from the PNNL database:

$$Enrichment = \frac{A_{ATR}}{A_{transmission}} = \frac{\varepsilon \cdot c_{film} \cdot d_{e,eff}}{\varepsilon \cdot c_{gas} \cdot d_{e,eff}} \qquad (2)$$

Assuming the same absorption coefficient ε for the area of a given band in condensed and gas phase, the enrichment factor also corresponds to the ratio of the volumetric concentrations c_{film} *and* c_{gas} (mol L^{-1}) in the mesoporous film and the gas. The enrichment factors obtained for 10 ppmv are 9600, 20480 and 32770 for toluene, *p*-xylene and 1,2,4-trimethylbenzene, respectively. Note that for higher concentrations the enrichment factor is lower due to the non-linearity of the calibration functions. The highest enrichment factor was found for 1,2,4-trimethylbenzene, the VOC with the lowest saturation vapor pressure and hence highest affinity to condense at surfaces, while toluene, having the highest saturation vapor pressure, yielded the lowest enrichment factor.

3.3. Multicomponent Sensing

A VOC mixture was prepared by inserting the premixed VOC solution into the gas container. With the same fitting routine as for the single component calibrations, three Lorentzian profiles were fitted to the obtained spectra. The spectrum of a VOC mixture with 146 ± 10 ppmv toluene, 151 ± 10 ppmv *p*-xylene and 58 ± 10 ppmv 1,2,4-trimethylbenzene adsorbed into the mesoporous silica film prepared using CTAB and the corresponding Lorentzian profiles are depicted in Figure 4. The obtained profile areas were inserted into the calibration function with parameters given in Table 1. The so found concentrations of 153 ± 15 ppmv toluene, 143 ± 12 ppmv *p*-xylene and 52 ± 8 ppm 1,2,4-trimethylbenzene are in very good agreement with the applied concentrations.

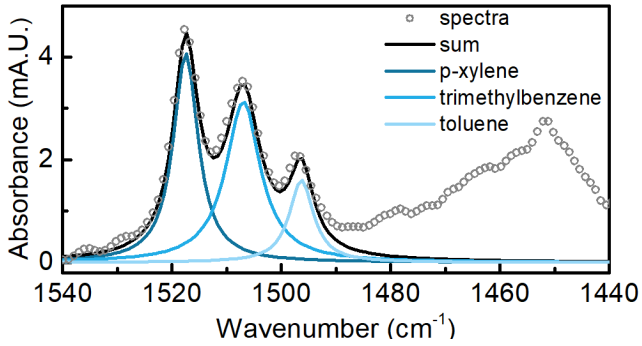

Figure 4. FTIR spectra of a mixture of VOC enriched on the mesoporous silica film prepared using CTAB with deconvolution using Lorentzian curves.

In a next step, this gas mixture was humidified by bubbling the stream of N_2 through water at 25 °C prior to mixing with the stream of diluted VOC from the pressure vessel. The thereby obtained gas transmission spectrum for 15 % humidity and 277 ± 10 ppmv toluene, 232 ± 10 ppmv *p*-xylene and 82 ± 10 ppmv trimethylbenzene given in Figure 5A shows the broad P and R branches of the water vapor deformation band. The VOCs' absorption bands present in the mixture are practically indistinguishable from the large

water background. The humidified gas mixtures were then applied to the mesoporous silica film prepared using CTAB and the spectrum is depicted in Figure 5B.

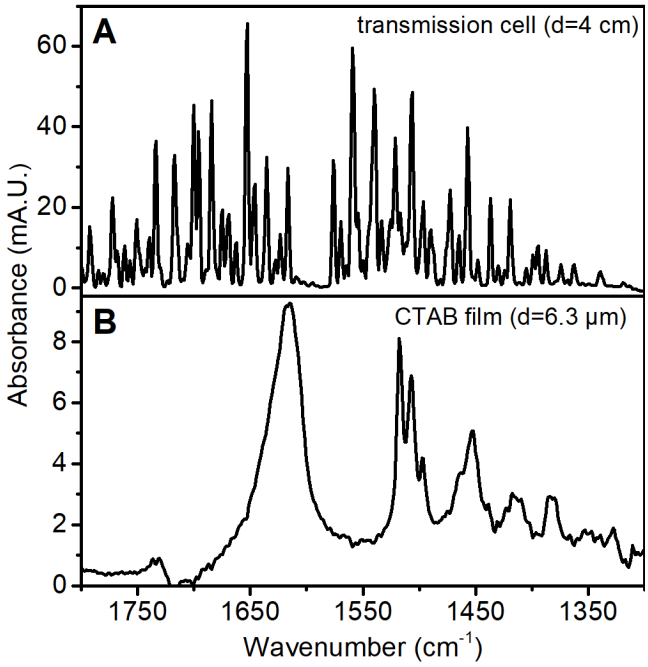

Figure 5. FTIR spectra of a mixture of VOC in humidified air obtained from a transmission measurement (A) and adsorbed to the mesoporous silica film produced using CTAB (B).

In addition to the well resolved VOC bands around 1500 cm^{-1}, a band of condensed water at 1620 cm^{-1} is visible. Since the film thickness of 400 nm largely covers the evanescent field, no bands associated with water vapor are present allowing for quantitative analysis of the adsorbed VOCs. The gas mixture was further mixed with humidified N_2 to yield a relative humidity up to 60 % and the findings for a concentration range between 25 - 300 ppmv VOC with varying relative humidity between 60 % and 15 % is given in Figure 6 (see ESI for all values). Here, the high humidity does not interfere with the measurement and the applied concentrations are in excellent agreement with the found VOC concentrations.

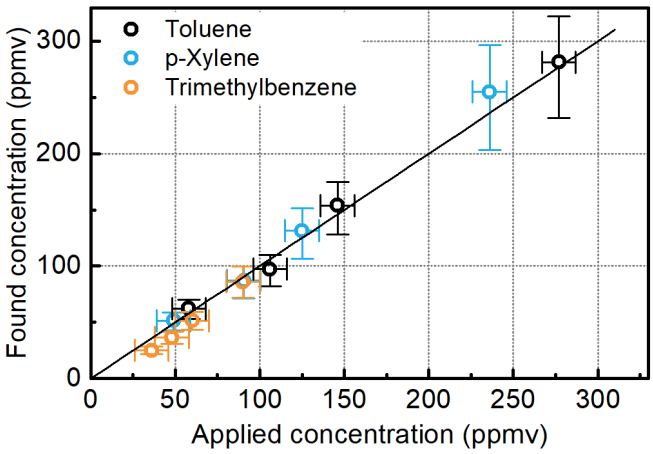

Figure 6. Found and applied concentrations for VOC mixtures on mesoporous silica film produced using CTAB from calibration.

4. Conclusion and Outlook

In this contribution, we introduced mesoporous silica films as enrichment material for VOC gas sensing. Mesoporous silica films with three different pore sizes between 5 - 12.5 nm were coated on Si ATR crystals and their sensing performance was evaluated using FTIR spectroscopy. The film with the smallest pore size clearly stood out and reached enrichment factors between 9000 up to 32 000, depending on VOC and corresponding saturation vapor pressure. Moreover, limits of detection as low as 3 - 7 ppmv with solely 6.3 µm effective path length were achieved. The remarkable increase in sensitivity was also reached in high-humidity atmosphere, which was enabled by organic functionalization of the mesoporous silica to largely exclude water interferences. The combination of these coatings with integrated optics and waveguide platforms of increased effective path length coupled with mid-IR light sources and detectors decreasing in size constantly holds great promise for highly sensitive detection of VOCs.

ASSOCIATED CONTENT

Supporting Information

IR spectra and X-ray diffraction patterns of mesoporous films are given in the Supporting Information

AUTHOR INFORMATION

Corresponding Author

*Email: bernhard.lendl@tuwien.ac.at

Author Contributions

All authors have given approval to the final version of the manuscript.

ACKNOWLEDGMENTS

This work is part of the AQUARIUS project, which has received funding from the European Union's Horizon 2020 research and innovation program under grant agreement No. 731465. This project is an initiative of the Photonics Public Private Partnership. J.H. acknowledges funding from the Competence Centre ASSIC – Austrian Smart Systems Integration Research Center – within the COMET – Competence Centers for Excellent Technologies program. X-ray diffraction was performed at the interfaculty X-Ray Center of TU Vienna.

References

1. Jia, C., Batterman, S. & Godwin, C. VOCs in industrial, urban and suburban neighborhoods, Part 1: Indoor and outdoor concentrations, variation, and risk drivers. *Atmos. Environ.* **42**, 2083–2100 (2008).
2. Guo, H., Lee, S. C., Chan, L. Y. & Li, W. M. Risk assessment of exposure to volatile organic compounds in different indoor environments. *Environ. Res.* **94**, 57–66 (2004).
3. Destaillats, H., Maddalena, R. L., Singer, B. C., Hodgson, A. T. & McKone, T. E. Indoor pollutants emitted by office equipment: A review of reported data and information needs. *Atmospheric Environment* **42**, 1371–1388 (2008).
4. Lee, C. W., Dai, Y. T., Chien, C. H. & Hsu, D. J. Characteristics and health impacts of volatile organic compounds in photocopy centers. *Environ. Res.* **100**, 139–149 (2006).
5. Spinelle, L., Gerboles, M., Kok, G., Persijn, S. & Sauerwald, T. Review of portable and low-cost sensors for the ambient air monitoring of benzene and other volatile organic compounds. *Sensors* **17**, 1–30 (2017).
6. HASEGAWA, T. *Quantitative infrared spectroscopy for understanding of a condensed matter*. *Springer Japan* (Springer Japan, 2017). doi:10.1007/978-4-431-56493-5
7. Sydoryk, I., Lim, A., Jäger, W., Tulip, J. & Parsons, M. T. Detection of benzene and toluene gases using a mid-infrared continuous-wave external cavity quantum cascade laser at atmospheric pressure. *Appl. Opt.* **49**, 945 (2010).
8. Young, C. R., Menegazzo, N., Riley, A. E., Brons, C. H., Disanzo, F. P., Givens, J. L., Martin, J. L., Disko, M. M. & Mizaikoff, B. Infrared hollow waveguide sensors for simultaneous gas phase detection of benzene, toluene, and xylenes in field environments. *Anal. Chem.* **83**, 6141–6147 (2011).
9. Sieger, M. & Mizaikoff, B. Toward On-Chip Mid-Infrared Sensors. *Anal. Chem.* **88**, 5562–5573 (2016).

10. Mizaikoff, B. Waveguide-enhanced mid-infrared chem/bio sensors. *Chem. Soc. Rev.* **42**, 8683 (2013).

11. Thompson, B. T., Inberg, A., Croitoru, N. & Mizaikoff, B. Characterization of a Mid-Infrared Hollow Waveguide Gas Cell for the Analysis of Carbon Monoxide and Nitric Oxide. *Appl. Spectrosc.* **60**, 266–271 (2006).

12. Soref, R. Mid-infrared photonics in silicon and germanium. *Nat. Photonics* **4**, 495–497 (2010).

13. Kita, D. M., Miranda, B., Favela, D., Bono, D., Michon, J., Lin, H., Gu, T. & Hu, J. High-performance and scalable on-chip digital Fourier transform spectroscopy. *Nat. Commun.* **9**, 4405 (2018).

14. Miller, S. A., Yu, M., Ji, X., Griffith, A. G., Cardenas, J., Gaeta, A. L. & Lipson, M. Low-loss silicon platform for broadband mid-infrared photonics. *Optica* **4**, 707–712 (2017).

15. Schwarz, B., Reininger, P., Ristanić, D., Detz, H., Andrews, A. M., Schrenk, W. & Strasser, G. Monolithically integrated mid-infrared lab-on-a-chip using plasmonics and quantum cascade structures. *Nat. Commun.* **5:4085**, (2014).

16. Kumari, B., Barh, A., Varshney, R. K. & Pal, B. P. Silicon-on-nitride slot waveguide: A promising platform as mid-IR trace gas sensor. *Sensors Actuators B Chem.* **236**, 759–764 (2016).

17. Liu, Q., Ramirez, J. M., Vakarin, V., Le Roux, X., Ballabio, A., Frigerio, J., Chrastina, D., Isella, G., Bouville, D., Vivien, L., Ramos, C. A. & Marris-Morini, D. Mid-infrared sensing between 5.2 and 6.6 μm wavelengths using Ge-rich SiGe waveguides. *Opt. Mater. Express* **8**, 1305–1312 (2018).

18. Robinson, J. T., Chen, L. & Lipson, M. On-chip gas detection in silicon optical microcavities. in *2008 Conference on Quantum Electronics and Laser Science Conference on Lasers and Electro-Optics, CLEO/QELS* **16**, 4296 (Optical Society of America, 2008).

19. Muneeb, M., Chen, X., Verheyen, P., Lepage, G., Pathak, S., Ryckeboer, E., Malik, A., Kuyken, B., Nedeljkovic, M., Van Campenhout, J., Mashanovich, G. Z. & Roelkens, G. Demonstration of Silicon-on-insulator mid-infrared spectrometers operating at 3.8μm. *Opt. Express* **21**, 11659–11669 (2013).

20. Yu, M., Okawachi, Y., Griffith, A. G., Picqué, N., Lipson, M. & Gaeta, A. L. Silicon-chip-based mid-infrared dual-comb spectroscopy. *Nat. Commun.* **9**, 1869 (2018).

21. Holmstrom, S. A., Stievater, T. H., Kozak, D. A., Pruessner, M. W., Tyndall, N., Rabinovich, W. S., Andrew McGill, R. & Khurgin, J. B. Trace gas Raman spectroscopy using functionalized waveguides. *Optica* **3**, 891–896 (2016).

22. Tyndall, N. F., Stievater, T. H., Kozak, D. A., Koo, K., McGill, R. A., Pruessner, M. W., Rabinovich, W. S. & Holmstrom, S. A. Waveguide-enhanced Raman spectroscopy of trace chemical warfare agent simulants. *Opt. Lett.* **43**, 4803–4806 (2018).

23. Vasiliev, A., Malik, A., Muneeb, M., Kuyken, B., Baets, R. & Roelkens, G. On-Chip Mid-Infrared Photothermal Spectroscopy Using Suspended Silicon-on-Insulator Microring Resonators. *ACS Sensors* **1**, 1301–1307 (2016).

24. Ramirez, J. M., Liu, Q., Vakarin, V., Frigerio, J., Ballabio, A., Le Roux, X., Bouville, D., Vivien, L., Isella, G. & Marris-Morini, D. Graded SiGe waveguides with broadband low-loss propagation in the mid infrared. *Opt. Express* **26**, 870–877 (2018).

25. Younis, U., Luo, X., Dong, B., Huang, L., Vanga, S., Lim, E.-J., Lo, G.-Q., Lee, C., Bettiol, A. A. & Ang, K.-W. Towards low-loss waveguides in SOI and Ge-on-SOI for mid-IR sensing. *J. Phys. Commun.* **2**, 045029 (2018).

26. Mashanovich, G. Z., Mitchell, C. J., Penades, J. S., Khokhar, A. Z., Littlejohns, C. G., Cao, W., Qu, Z., Stanković, S., Gardes, F. Y., Masaud, T. Ben, Chong, H. M. H., Mittal, V., Murugan, G. S., Wilkinson, J. S., Peacock, A. C. & Nedeljkovic, M. Germanium Mid-Infrared Photonic Devices. *J. Light. Technol.* **35**, 624–630 (2017).

27. Chang, Y.-C., Paeder, V., Hvozdara, L., Hartmann, J.-M. & Herzig, H. P. Low-loss germanium strip waveguides on silicon for the mid-infrared. *Opt. Lett.* **37**, 2883–2885 (2012).

28. Lu, R., Sheng, G., Li, W., Yu, H., Raichlin, Y., Katzir, A. & Mizaikoff, B. IR-ATR chemical sensors based on planar silver halide waveguides coated with an ethylene/propylene copolymer for detection of multiple organic contaminants in water. *Angew. Chemie - Int. Ed.* **52**, 2265–2268 (2013).

29. Stach, R., Pejcic, B., Crooke, E., Myers, M. & Mizaikoff, B. Mid-Infrared Spectroscopic Method for the Identification and Quantification of Dissolved Oil Components in Marine Environments. *Anal. Chem.* **87**, 12306–12312 (2015).

30. Lamotte, M., De Violet, P., Garrigues, P. & Hardy, M. Evaluation of the possibility of detecting benzenic pollutants by direct spectrophotometry on PDMS solid absorbent. *Anal. Bioanal. Chem.* **372**, 169–173 (2002).

31. Lu, Y., Han, L., Brinker, C. J., Niemczyk, T. M. & Lopez, G. P. Chemical sensors based on hydrophobic porous sol-gel films and ATR-FTIR spectroscopy. *Sensors Actuators B Chem.* **36**, 517–521 (1996).

32. Baumgartner, B., Hayden, J., Schwaighofer, A. & Lendl, B. In Situ IR Spectroscopy of Mesoporous Silica Films for Monitoring Adsorption Processes and Trace Analysis. *ACS Appl. Nano Mater.* **1**, 7083–7091 (2018).

33. Wang, Z., Larsson, M. L., Grahn, M., Holmgren, A. & Hedlund, J. Zeolite coated ATR crystals for new applications in FTIR-ATR spectroscopy. *Chem. Commun.* 2888–2889 (2004). doi:10.1039/b410314a

34. Grahn, M., Holmgren, A. & Hedlund, J. Adsorption of n-hexane and p-xylene in thin silicalite-1 films studied by FTIR/ATR spectroscopy. *J. Phys. Chem. C* **112**, 7717–7724 (2008).

35. Huang, G. G., Wang, C., Tang, H., Huang, Y. & Yang, J. ZnO Nanoparticle-Modified Infrared Internal Reflection Elements for Selective Detection of Volatile Organic Compounds functional groups were observed . The conditions for were optimized by varying such factors as the volume of. *Anal. Chem.* **78**, 2397–2404 (2006).

36. Gibson, L. T. Mesosilica materials and organic pollutant adsorption: Part A removal from air. *Chemical Society Reviews* **43**, 5163–5172 (2014).

37. Kosuge, K., Kubo, S., Kikukawa, N. & Takemori, M. Effect of pore structure in mesoporous silicas on VOC dynamic adsorption/desorption performance. *Langmuir* **23**, 3095–3102 (2007).

38. Wagner, T., Haffer, S., Weinberger, C., Klaus, D. & Tiemann, M. Mesoporous materials as gas sensors. *Chemical Society Reviews* **42**, 4036–4053 (2013).

39. Soler-Illia, G. J. D. A. A., Sanchez, C., Lebeau, B. & Patarin, J. Chemical strategies to design textured materials: From microporous and mesoporous oxides to nanonetworks and hierarchical structures.

Chem. Rev. **102**, 4093–4138 (2002).

40. Innocenzi, P. & Malfatti, L. Mesoporous thin films: properties and applications. *Chem. Soc. Rev.* **42**, 4198–4216 (2013).

41. Zhao, H., Raza, A., Baumgartner, B., Clemmen, S., Lendl, B., Skirtach, A. & Baets, R. Waveguide-Enhanced Raman Spectroscopy Using a Mesoporous Silica Sorbent Layer for Volatile Organic Compound (VOC) Sensing. in *Conference on Lasers and Electro-Optics* STh1F.7 (OSA, 2019). doi:10.1364/cleo_si.2019.sth1f.7

42. Bourda, L., Jena, H. S., Van Deun, R., Kaczmarek, A. M. & Van Der Voort, P. Functionalized periodic mesoporous organosilicas: From metal free catalysis to sensing. *J. Mater. Chem. A* **7**, 14060–14069 (2019).

43. Zheng, Q., Zhu, Y., Xu, J., Cheng, Z., Li, H. & Li, X. Fluoroalcohol and fluorinated-phenol derivatives functionalized mesoporous SBA-15 hybrids: high-performance gas sensing toward nerve agent. *J. Mater. Chem.* **22**, 2263 (2012).

44. Ramer, G. & Lendl, B. Attenuated Total Reflection Fourier Transform Infrared Spectroscopy. in *Encyclopedia of Analytical Chemistry* (John Wiley & Sons, Ltd, 2013).

45. Brinker, J. C., Lu, Y., Sellinger, A. & Fan, H. Evaporation-Induced Self-Assembly: Nanostructures Made Easy. *Adv. Mater.* **11**, 579–585 (1999).

46. Baumgartner, B., Hayden, J., Loizillon, J., Steinbacher, S., Grosso, D. & Lendl, B. Pore Size-Dependent Structure of Confined Water in Mesoporous Silica Films from Water Adsorption-Desorption using ATR-FTIR Spectroscopy. *Langmuir* (2019). doi:10.1021/acs.langmuir.9b01435

47. Barczak, M. Template removal from mesoporous silicas using different methods as a tool for adjusting their properties. *New J. Chem.* **42**, 4182–4191 (2018).

48. Baumgartner, B., Hayden, J., Loizillon, J., Steinbacher, S., Grosso, D. & Lendl, B. Pore Size-Dependent Structure of Confined Water in Mesoporous Silica Films from Water Adsorption/Desorption Using ATR–FTIR Spectroscopy. *Langmuir* **35**, 11986–11994 (2019).

49. Jelassi, J., Grosz, T., Bako, I., Bellissent-Funel, M.-C., Dore, J. C., Castricum, H. L. & Sridi-Dorbez, R. Structural studies of water in hydrophilic and hydrophobic mesoporous silicas: An x-ray and neutron diffraction study at 297 K. *J. Chem. Phys.* **134**, 064509 (2011).

50. Liu, Y. & Ojamäe, L. Raman and IR Spectra of Ice Ih and Ice XI with an Assessment of DFT Methods. *J. Phys. Chem. B* **120**, 11043–11051 (2016).

51. Neimark, A. V., Thommes, M., Sing, K. S. W., Rodriguez-Reinoso, F., Olivier, J. P., Kaneko, K. & Rouquerol, J. Physisorption of gases, with special reference to the evaluation of surface area and pore size distribution (IUPAC Technical Report). *Pure Appl. Chem.* **87**, (2015).